*J. Fluid Mech.* (2003), *vol.* 491, *pp.* 353–378.  
DOI: 10.1017/S0022112003005548 Printed in the United Kingdom

# Anisotropy and energy flux in wall turbulence

By D. C. DUNN† AND J. F. MORRISON
Department of Aeronautics, Imperial College, London SW7 2AZ, UK

(Received 20 June 2002 and in revised form 5 March 2003)

A term-by-term wavelet decomposition of the equation for turbulence kinetic energy in turbulent channel flow is used to provide a dual space-scale description of the production and flux of energy. Wavelet filtering, analogous to that used in large-eddy simulation, is performed on the nonlinear term that constitutes the energy flux. Meneveau's term, $\pi_{sg}^{(m)}[\boldsymbol{i}]$ is used to represent forward scatter and backscatter. This term is highly intermittent, much more so than the equivalent terms for production at the same scale. Virtually all of $\pi_{sg}^{(m)}[\boldsymbol{i}]$ appears in only two components that involve subgrid flux of streamwise momentum in the wall-normal and spanwise directions. An equivalent term that is the wavelet transform of the pressure-gradient term is shown to be several orders of magnitude smaller, consistent with its neglect in current subgrid modelling techniques. However, the mean-square pressure-gradient fluctuations (that reach a maximum in the range of wavenumbers in which the velocity spectra exhibit a $-5/3$ slope) are responsible for the significant spatial intermittency observed in the energy flux.

## 1. Introduction

One of the most intractable problems in large-eddy-simulation (LES) is the modelling of turbulence affected by a solid surface, in terms of both the modelling of the unresolved scales that are smaller than the filter or grid size (the 'subgrid' scales) and the implementation of an appropriate surface condition. This arises because near a surface all the scales are 'small' so that the energy-containing scales may be smaller than the grid size. Moreover, grid requirements make the use of approximate 'off-the-surface' boundary conditions very attractive (e.g. Piomelli & Balaras 2002). Subgrid-scale (SGS) modelling is particularly difficult near solid surfaces where the energy spectrum becomes complicated by the prevalence there of 'backscatter', the transfer of energy away from the small scales to the large ones. Meneveau (1994) has discussed which statistics a SGS model should reproduce in order to be considered sound. Such quantities include the low-order statistics of the energy transfer. Popular eddy-viscosity models present difficulties because they are absolutely dissipative: Mason & Thomson (1992), for example, show that only with the use of a stochastic backscatter model can the log law be obtained accurately when it is used as a time-dependent surface boundary condition. The dynamic model of Germano *et al.* (1991) also presents problems concerning backscatter although Porté-Agel, Meneveau & Parlange (2000) have generalized the model to improve predictions of a neutral atmospheric surface layer. Recent attempts by Redelsperger, Mahé & Carlotti (2001) to use SGS models based on the supposed self-similarity of surface-parallel velocity

† Present address: School of Mathematics, University of Bristol, University Walk, Bristol BS8 1TW, UK.

spectra as a function of streamwise wavenumber may lack generality: Morrison *et al.* (2002*b*) have shown that spectra of the streamwise velocity component do not exhibit self-similarity even at very high Reynolds numbers. Further difficulties arise in the definition of a suitable SGS lengthscale, which is usually related simply to the grid size. The grid must have very large aspect ratios in order that the essential properties of the turbulence are captured (Ferziger & Perić 1996), but a model with a single lengthscale is unlikely to represent spectral transfer in wall turbulence accurately. Anisotropy of the turbulence near the wall extends to anisotropy in the SGS stresses.

Further difficulties stem from the fact that, in order to obtain the required level of detail, some surface models are developed using linear stochastic estimation applied to simulation databases (e.g. Nicoud *et al.* 2001). But Morrison *et al.* (2002*a*) have recently demonstrated that the anisotropy of near-wall turbulence increases as the Reynolds number increases. This is due to the anisotropy of turbulence structures induced by the mean shear: Robinson (1991) shows that in wall turbulence, quasi-streamwise vortices are typically 1000 viscous units long, while they are only 30–50 viscous units in diameter. A structure-based model of wall turbulence must surely embody these effects, but it is by no means clear which turbulence structures are responsible for spectral transfer. Robinson (1991) shows that, at low Reynolds number, spatial transport is largely caused by the circulation of quasi-streamwise vortices, in terms either of 'ejections' of low-momentum fluid away from the wall, or of 'sweeps' of high-momentum fluid towards the wall. Our own view is coloured largely by the experimental results of Morrison, Subramanian & Bradshaw (1992) who suggest that ejections and sweeps in the local-equilibrium region constitute a 'first-order' inertial subrange, a sufficient criterion for which is that energy sources or sinks are a small fraction of the energy transfer. Formally, this does not require local isotropy in a wavenumber range in which the spectral shear correlation coefficient may be expected to be rapidly decreasing with increasing wavenumber (Saddoughi & Veeravalli 1994). Bradshaw (1967) suggests a suitable criterion for a first-order subrange is that the Taylor microscale Reynolds number, $R_\lambda > 100$. This is a much less stringent condition than local isotropy, which Durbin & Speziale (1991) show is not justifiable even at high Reynolds numbers if the mean rate of strain is not small. For these reasons, we refer to a spectral region in which the cutoff is placed to be one in which the slope is $-5/3$, rather than making explicit reference to a supposed inertial subrange.

There has been extensive research concerning backscatter and its relevance to the dynamics of the viscous sublayer (see Piomelli, Yu & Adrian 1996; Härtel & Kleiser 1998; Domaradzki *et al.* 1994). The origin of this reverse cascade is of fundamental interest, not only for LES modelling, but also for control of turbulence in engineering applications. In fact, such results are relevant to any small-scale forcing. Härtel *et al.* (1994), Härtel & Kleiser (1998) and Domaradzki *et al.* (1994) have undertaken *a priori* studies of the subgrid-scale energy transfer using the quantities derived from the filtered Navier–Stokes equations. The drawback of this approach is that only the bulk transfer between the resolved and subgrid-scale motion is calculated, i.e. there is no reference to which of the resolved scales are involved in the transfer. Härtel & Kleiser (1998) and Piomelli *et al.* (1996) have suggested that sweeps and ejections play a critical role in energy transfer. More recently, Akhavan *et al.* (2000) have suggested that spectral energy transfers in a free jet comprise two effects: one involves forward scatter from non-local interactions that could suitably be modelled by eddy viscosity; the other involves local interactions around the cutoff generating bi-directional transfers. They suggest that this latter effect arises due to the presence of organized vortical structures, and owing to their coherent and scale-dependent

nature, the energy transfer is unlikely to be modelled successfully by a stochastic force (e.g. Mason & Thomson 1992).

From the foregoing, it is clear that a dual space-scale description of the energy processes in wall turbulence is called for. Orthogonal wavelets provide a compromise between the two descriptions. Here we use the orthogonal wavelet transform of the Navier–Stokes equations for fully developed turbulent channel flow applied to direct-simulation databases. For generality, we use the term 'flux' to describe the mixed spatial transport and scale-to-scale transfer of energy. Such a decomposition has been suggested by Meneveau (1991) who analysed (largely) the decay of isotropic turbulence and homogeneous turbulence subject to mean shear. Meneveau (1991) concentrated on flux quantities derived from the nonlinear and pressure-gradient terms. Here we take the analysis further and concentrate not only on the flux term, but also on the production of turbulence kinetic energy. In addition to the corresponding viscous term, these terms were identified by Dunn & Morrison (2003) who show that both the production and viscous terms occur across a range of scales and are intermittent. However, the greatest intermittency appears in the flux term. See also Dunn & Morrison (2000*a*, *b*, 2001) for fuller descriptions and earlier results.

Here, our examination of the nonlinear and pressure-gradients terms separately leads to some important conclusions. Moreover, in recognition of the pronounced anisotropy of wall turbulence, individual components of the non-linear term are examined. Given that most of the energy enters the turbulence via the streamwise velocity component and is redistributed by pressure fluctutations (strictly, the pressure–strain terms), we also investigate the role of pressure fluctuations in the wavelet domain. The mixed space-scale description offered by orthonormal wavelets is also a useful tool for investigating the relationship between energy flux and other simpler flow scalars representative of flow structure, but this is reported elsewhere. Preliminary studies using the wavelet representation have been undertaken by Westbury & Sandham (1996) and Westbury, Sandham & Morrison (1998), who show at least a qualitative relationship between regions of significant energy flux and sweeps and ejections. The aim of this paper is to elucidate and quantify (at least in some average sense) the effects of anisotropy on the flux of energy and this is done by a further decomposition of the dominant flux quantities. However, the present work also highlights a principal limitation of the orthonormal wavelet algorithm used here, namely the loss of 'identity' between the wavelet quantities and the primitive variables of the DNS database used to define them.

In the next section, we briefly summarize those quantities used in LES that are relevant to the present work. Section 3 offers a brief review of the wavelet technique and summarizes results that aid description of the DNS databases. Section 4 outlines a decomposition that defines the SGS stresses and subsequent sections provide results for the production and flux quantities.

## 2. LES equations

The LES equations are obtained by applying a low-pass filter to the Navier–Stokes equations (the filter must commute with differentiation; see e.g. Leonard 1974; Lund 1997). Decomposing a flow variable $f = \tilde{f} + f'$, where $\tilde{f}$ is the filtered variable, the Navier–Stokes equations become

$$\frac{\partial \tilde{u}_i}{\partial t} + \frac{\partial \tilde{u}_i \tilde{u}_j}{\partial x_j} = -\frac{1}{\rho}\frac{\partial \tilde{p}}{\partial x_i} - \frac{\partial \tau_{ij}}{\partial x_j} + \nu \frac{\partial^2 \tilde{u}_i}{\partial x_j \partial x_j}, \qquad \frac{\partial \tilde{u}_i}{\partial x_i} = 0. \tag{2.1a, b}$$

The unknown terms, which require modelling, are the subgrid-scale (SGS) stresses

$$\tau_{ij} = \widetilde{u_i u_j} - \tilde{u}_i \tilde{u}_j. \tag{2.2}$$

In the balance equation for the grid-scale (GS) kinetic energy $\tau_{kk}$, the term representing the exchange of energy between the resolved and subgrid scales is

$$\epsilon_{sg} = \tilde{u}_i \frac{\partial}{\partial x_j} \tau_{ij} = \frac{\partial}{\partial x_j} \tilde{u}_i \tau_{ij} - \tau_{ij} \tilde{S}_{ij}, \tag{2.3}$$

where the resolved-scale strain-rate tensor is

$$\tilde{S}_{ij} = \frac{1}{2} \left( \frac{\partial \tilde{u}_i}{\partial x_j} + \frac{\partial \tilde{u}_j}{\partial x_i} \right). \tag{2.4}$$

The terms on the right-hand side of (2.3) are the SGS diffusion and the SGS dissipation, both of which appear in the equation for the GS kinetic energy (e.g. Piomelli *et al.* 1996). The SGS diffusion represents a spatial redistribution of GS energy by the SGS motion, whereas the SGS dissipation, $T = -\tau_{ij} \tilde{S}_{ij}$, represents a true source or sink of GS energy. Piomelli *et al.* (1996) reason that the SGS model should reproduce the SGS dissipation, but not necessarily the diffusion.

The present analysis uses DNS channel flow data (Sandham & Howard 1995) at Reynolds number, $Re_\tau = 300$ (based on the friction velocity, $u_\tau$, and channel half-height $\delta$). The computational domain is $13\delta \times 2\delta \times 6\delta$ in the $x$- (streamwise, $i = 1$), $y$- (wall-normal, $i = 2$) and $z$- (spanwise, $i = 3$) directions respectively. The grid spacings in the $x$- and $z$-directions are uniform, while those in the $y$-direction are finer closer to the wall. In the following, superscript $^+$ denotes scaling in wall units. The data are analysed in two-dimensional, homogeneous $(x, z)$-planes. This is not anticipated to lead to spurious results, except perhaps in the linear sublayer: Murray, Piomelli & Wallace (1996) have shown that two-dimensional filtering (using a Fourier cutoff filter) is equivalent to three-dimensional filtering only for $y^+ > 10$.

Leaving aside the more pragmatic details of wall modelling for LES at high Reynolds number, and taking $y^+$ to be a local Reynolds number, it is clear that the energy flux as deduced from DNS databases is relevant to flows with much higher bulk Reynolds numbers. However, by any standard, the Reynolds number is 'low' and, particularly in the context of energy flux, this should be dealt with in the analysis. Härtel *et al.* (1994) and Härtel & Kleiser (1998) investigate low-Reynolds-number effects in near-wall turbulence, and their decomposition is briefly reviewed here. The SGS dissipation is decomposed by dividing the subgrid-scale stresses into a statistically stationary mean value, $\langle \tau_{ij} \rangle$, here averaged over homogeneous planes, and a fluctuating part, $\tau'_{ij}$, so that

$$T = T^{ms} + T^{fs}, \tag{2.5}$$

where

$$T^{ms} = -\langle \tau_{ij} \rangle \langle \tilde{S}_{ij} \rangle, \quad T^{fs} = -\langle \tau'_{ij} \tilde{S}'_{ij} \rangle. \tag{2.6a, b}$$

Here $T^{ms}$ represents kinetic energy production in the SGS motion and $T^{fs}$ represents a redistribution of kinetic energy within the turbulence spectrum. In ideal high-Reynolds-number LES modelling (figure 1), the following relationships hold:

$$T^{fs} = \epsilon, \quad T^{ms} = 0, \quad \epsilon_\nu = 0, \tag{2.7}$$

where $\epsilon_\nu = \nu \langle \tilde{S}'^2_{ij} \rangle$ is the mean viscous dissipation in the GS motion. In the case of low Reynolds number (figure 2), the wavenumbers at which production occurs are

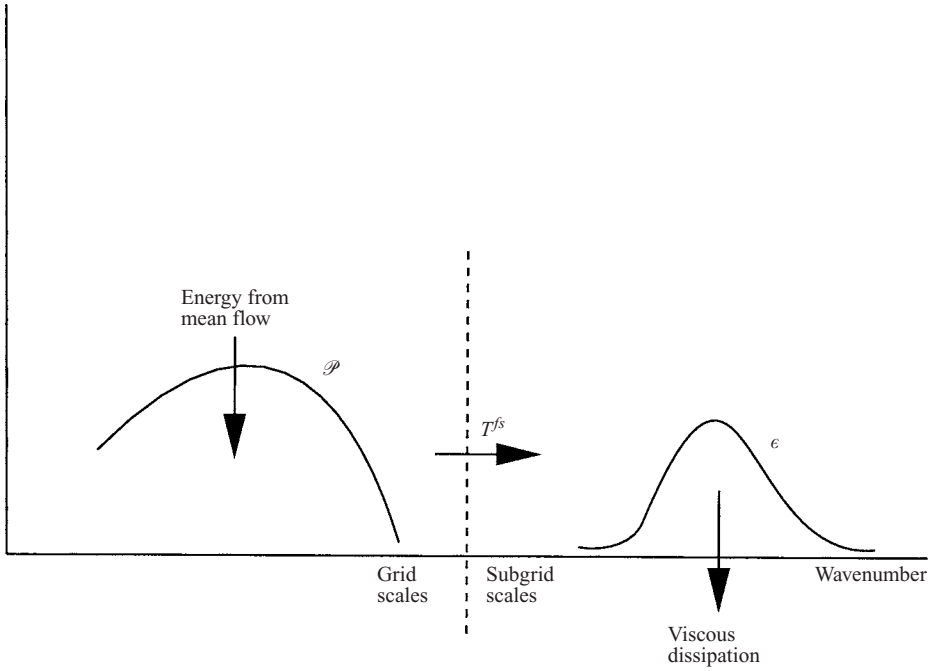


FIGURE 1. LES modelling in high-Reynolds-number flow. Production, $\mathscr{P}$, and dissipation, $\epsilon$, are well-separated in wavenumber space. The LES cutoff wavenumber lies in the inertial range and the effect of the subgrid-scale motion is to drain grid-scale energy at a rate $T^{fs} = \epsilon$.

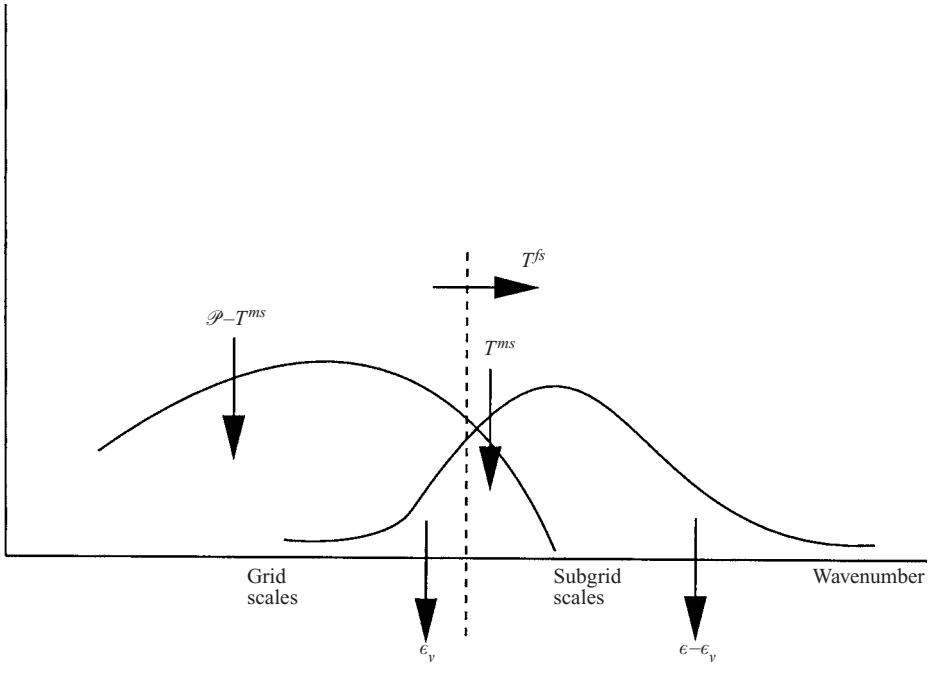


FIGURE 2. Schematic diagram of low-Reynolds-number flow. Prodution and dissipation are not separated in wavenumber space. Production occurs in the subgrid-scale motion ($T^{ms}$). There is viscous dissipation of grid-scale energy ($\epsilon_v$) and $T^{fs} < \epsilon$.

| $m$ | $r_m^+$ | $k_m\eta$ | $m$ | $r_m^+$ | $k_m\eta$ |
|---|---|---|---|---|---|
| 1 | 20.86 | 0.518 | 5 | 333.8 | 0.032 |
| 2 | 41.72 | 0.259 | 6 | 667.6 | 0.016 |
| 3 | 83.45 | 0.129 | 7 | 1335. | 0.008 |
| 4 | 166.9 | 0.065 | 8 | 2670. | 0.004 |

TABLE 1. Values for $r_m^+$ and $k_m\eta$ available for the wavelet analysis, at $Re_\tau = 300$. Here, the Kolmogorov length scale, $\eta$, has been calculated at $y^+ \approx 15$. In the remaining plots the full $y$-dependence of $\eta$ is retained.

not well separated from the dissipation range. In this case there is production in the subgrid scales, and viscous dissipation in the resolved scales. Low-Reynolds-number effects cause a decrease in the value of $T^{fs}$ relative to $\epsilon$. Dunn & Morrison (2003) show that production and viscous effects are present in all scales of the motion, and that both processes are very intermittent in space.

## 3. The wavelet transform

Mallat (1989) provides a fast wavelet algorithm, the details of which have appeared several times in the literature (for applications in turbulence, see e.g. Meneveau 1991; Do-Khac *et al.* 1994; Farge 1989). Like the Fourier transform, the square of the wavelet coefficients can be interpreted as the kinetic energy of the signal. The benefit of the wavelet transform is that it provides a description which is local in both scale *and* spatial location. Specifically, a function, $f(x, y)$, can be written

$$f(x, y) = \sum_{m=-\infty}^{\infty} \sum_{q=1}^{3} \sum_{\boldsymbol{i}} w^{(m,q)}[\boldsymbol{i}] \Psi^{(m,q)}[\boldsymbol{x} - 2^m \boldsymbol{i}], \tag{3.1}$$

where $[\boldsymbol{i}]$ is a variable two-dimensional position index. The basis functions $\Psi^{(m,q)}$ are generated by wavelet and smoothing functions, which have the shape of band-pass and low-pass filters respectively. The wavelet coefficients are

$$w^{(m,q)}[i_1, i_2] = \int_{-\infty}^{\infty} \int_{-\infty}^{\infty} f(x, y) \Psi^{(m,q)}[\boldsymbol{x} - 2^m \boldsymbol{i}] \, \mathrm{d}x \, \mathrm{d}y. \tag{3.2}$$

For a periodic signal on $2^M \times 2^M$ grid points, $2^{2(M-m)}$ wavelet coefficients can be obtained for $m = 1, \ldots, M$, corresponding to scales of a characteristic size $r_m = 2^m (\Delta_x \Delta_z)^{1/2}$, where $\Delta_x$ and $\Delta_z$ are the grid spacings (here streamwise and spanwise respectively). Table 1 shows the range of scales for the DNS databases. The wavenumber is $k_m = 2\pi / r_m$.

At higher wavenumber, the spatial localization is greater, but wavenumber localization is lost. This 'leakage' means that at large wavenumbers, the wavelet coefficients contain information from smaller wavenumbers. According to Qiu, Paw & Shaw (1995) the LeMarie–Meyer–Battle (LMB) wavelets minimize this effect. After Mallat (1989) and Meneveau (1991), LMB wavelets are also used for the present analysis.

Meneveau (1991) defines the energy spectral tensor,

$$E_{ij}(k_m) = \frac{2^{-m} (\Delta_x \Delta_z)^{1/2}}{\pi \sqrt{2}} \left\langle e_{ij}^{(m)}[\boldsymbol{i}] \right\rangle, \tag{3.3}$$

where the average is over all spatial locations, and

$$e_{ij}^{(m)}[\boldsymbol{i}] = \sum_{q=1}^{3} w_i^{(m,q)}[\boldsymbol{i}] w_j^{(m,q)}[\boldsymbol{i}]. \tag{3.4}$$

The two-dimensional energy spectrum is the trace of (3.3), and the total energy satisfies

$$\langle q \rangle = \sum_{m=1}^{M} E_{ii}^{(m)}(k_m) \Delta k_m. \tag{3.5}$$

Dunn & Morrison (2003) show $E_{ii}^{(m)}(k_m, y^+)$, together with the contributions by the various velocity components. The kinetic energy reaches a maximum at $y^+ \approx 15$, which coincides with the peak in turbulence kinetic energy production (e.g. Mansour, Kim & Moin 1988). The flow is highly anisotropic across the whole of the wall region, at all scales, including those near the viscous cutoff. The effect of this anisotropy on the exchange of energy between the GS and SGS motion is the subject of the rest of this paper.

## 4. SGS stress tensor based on wavelet filtering

It is straightforward to define low- and high-pass filtering operations based on the wavelet transform. The present analysis is that of Meneveau (1991), where details can be found. Here, the formulation is adapted for the channel flow data, and written to make the relationship with LES modelling explicit. A smoothed approximation (band-pass filtered) version, $u_i^{(m)}[\boldsymbol{i}]$, of the velocity field can be computed such that

$$u_i(\boldsymbol{x}) = \sum_{m=1}^{M} u_i^{(m)}[\boldsymbol{i}]. \tag{4.1}$$

The velocity field can be written,

$$u_i(\boldsymbol{x}) = u_i^{<m}(\boldsymbol{x}) + u_i^{>m}(\boldsymbol{x}), \tag{4.2}$$

where

$$u_i^{<m}[\boldsymbol{i}] = \sum_{n=1}^{m-1} u_i^{(n)}[\boldsymbol{i}], \quad u_i^{>m}[\boldsymbol{i}] = \sum_{n=m}^{M} u_i^{(n)}[\boldsymbol{i}]. \tag{4.3a,b}$$

In practice these quantities are calculated by setting to zero the wavelet coefficients at the scales to be ignored, and then inverting the transform. The operation can be thought of as a wavelet cutoff filter. The fields corresponding to (4.3*a*, *b*) are, respectively, high- and low-pass filtered velocity fields, similar to those produced by a Fourier cutoff filter, but with the filtering being 'local' in physical as well as wavenumber space. The '$> m$' and '$< m$' superscripts can be taken to represent 'grid-scale' and 'subgrid-scale' motion, respectively. Subgrid-scale stresses can be constructed:

$$\tau_{ij}^{(m)} = u_i u_j - u_i^{>m} u_j^{>m}. \tag{4.4}$$

Clearly, this definition is not quite the same as the SGS stresses defined by (2.2): while it yields all the cross-stresses and Reynolds stresses, as products they remain unfiltered, in contrast to the SGS stresses defined by (2.2). However, this difference is addressed in § 6 where we define a quantity that represents the flux of energy between

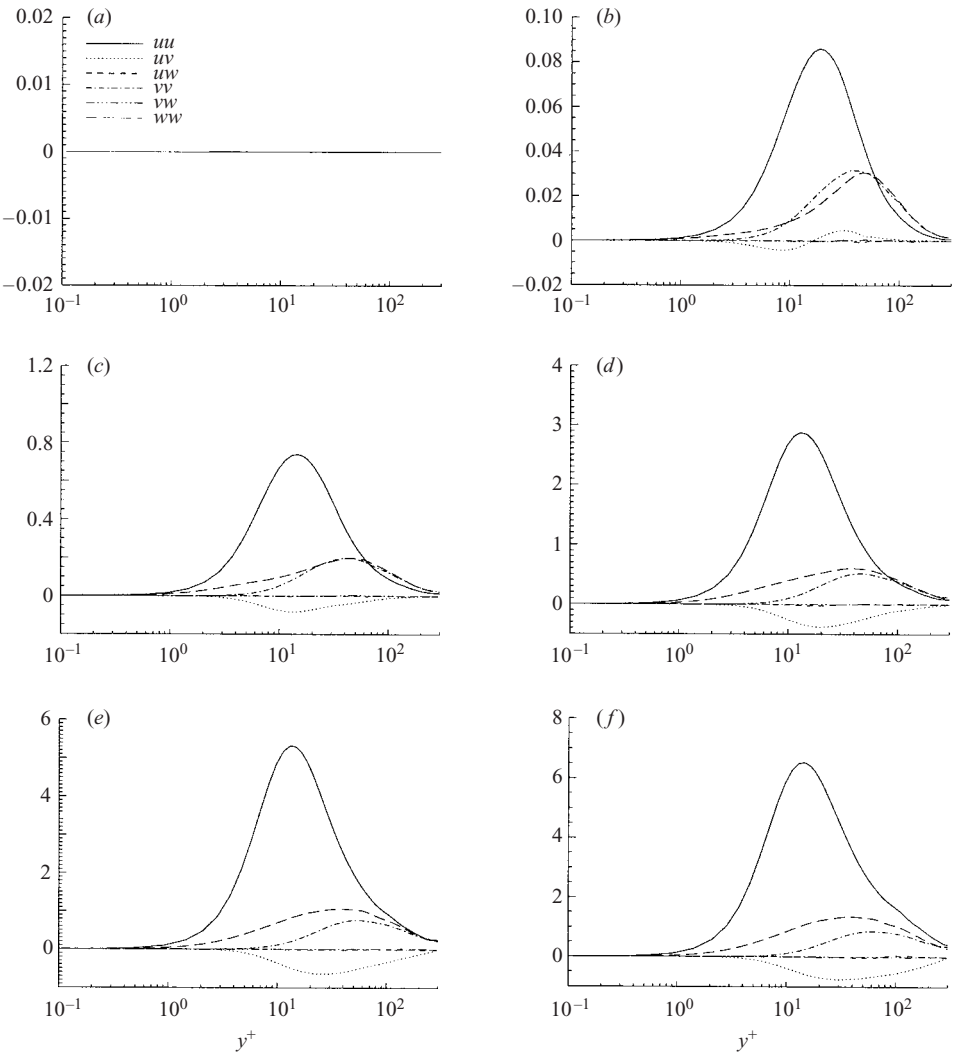


FIGURE 3. The components of the wavelet-based subgrid-scale stress tensor $\langle \tau_{ij}^{(m)} \rangle$. (*a*) $m = 1$, (*b*) 2, (*c*) 3, (*d*) 4, (*e*) 5, (*f*) 6. Note that the scale on the vertical axis varies between plots.

the GS and SGS motion. Figure 3 shows the mean values of the SGS stresses: those for $m = 3, 4$ and 5, correspond to wavenumbers lying in the $-5/3$ region, and so are most relevant to LES modelling. Only five of the nine terms are non-zero in the mean, i.e. the diagonal stresses and the stresses aligned with the mean strain rate, $\tau_{12}^{(m)} = \tau_{21}^{(m)}$. All of the terms show maxima (and/or minima) either in or just above the sublayer, indicating that a significant proportion of the turbulence kinetic energy is contained in the small scales. They also exhibit the expected anisotropy, the normal stress aligned in the streamwise direction being significantly larger than those in the wall-normal and spanwise directions. This behaviour is consistent with that of the Reynolds stresses (Dunn & Morrison 2003). Each of the SGS stress terms shows an increase with increasing $m$, i.e. as the filter width in Fourier space decreases. Therefore, the anisotropy of the Reynolds stresses that arises because of the different effects that

the viscous and impermeability constraints have on near-wall turbulence also appears in the SGS stresses, down to the viscous cutoff.

These curves are not directly comparable with the plots of the SGS stresses calculated by Härtel & Kleiser (1998), since, in order to retain a physical description, we have not subtracted out the isotropic part of the SGS stress tensor. This is usually done for consistency in eddy-viscosity modelling so that the SGS stresses are trace-free as is the resolved strain-rate tensor. It should also be noted that, because a wavelet filter produces SGS and GS scales that overlap in spectral space, the resulting components of the SGS stresses, (4.4), are not Galilean invariant. However, we do not separate the SGS stresses into those components that contain a plane-averaged velocity and those that do not. Therefore the question of Galilean invariance does not arise. Härtel & Kleiser (1997) deal with issues of Galilean invariance in detail. Moreover, Härtel & Kleiser (1998) show that, in terms of energy transfer, the cross-stresses and the SGS Reynolds stresses behave in a very similar fashion. It would therefore seem appropriate to model them together. What we will show however, is that the individual components of the SGS stress tensor behave very differently.

## 5. Energy production in wavelet space

While it is not possible to separate the SGS diffusion and dissipation in the othogonal wavelet representation (see below), it is possible to separate the mean flow effects from the flux due only to the turbulence. The term

$$P^{(m)}[\boldsymbol{i}] = \sum_{i=1}^{3}\sum_{q=1}^{3} w_i^{(m,q)}[\boldsymbol{i}] \left\{ u_j \frac{\partial U_i}{\partial x_j} \right\}^{(m,q)} [\boldsymbol{i}], \tag{5.1}$$

is the production of turbulence kinetic energy in a region of characteristic size $r_m$ at the point $[\boldsymbol{i}]$ (see Dunn & Morrison 2003). Here $\{\cdot\}^{(m,q)}[\boldsymbol{i}]$ denotes the wavelet coefficients of a quantity other than velocity. The spectrum of $P^{(m)}[\boldsymbol{i}]$ at fixed $y^+$ is

$$\mathscr{P}_w(y^+, k_m) = \frac{2^{-m}(\Delta_x\Delta_y)^{1/2}}{\pi\sqrt{2}} \langle P^{(m)}[\boldsymbol{i}] \rangle. \tag{5.2}$$

Figure 4 shows $\mathscr{P}_w(y^+, k_m)$ as a function of $y^+$. Summing $\mathscr{P}_w(y^+, k_m)\Delta k_m$ over all $m$ yields the total production of turbulence kinetic energy. For $m = 1$, corresponding to scales near the viscous cutoff, there is no production. However, across the rest of the range of scales production is significant. $\mathscr{P}_w$ has maxima close to $y^+ = 15$, but moves to slightly larger values of $y^+$ as $m$ increases. Maximum production occurs for $m = 4$, the region where a cutoff wavenumber might be selected for LES at high Reynolds numbers. Dunn & Morrison (2003) show that the wavelet-transformed viscous term also reaches a maximum at $m = 4$.

The standard deviation of $P^{(m)}[\boldsymbol{i}]$, in the same units as $\mathscr{P}_w$ is

$$\sigma_{\mathscr{P}}(y^+, k_m) = \frac{2^{-m}(\Delta_x\Delta_y)^{1/2}}{\pi\sqrt{2}} \left( \langle P^{(m)}[\boldsymbol{i}]^2 \rangle - \langle P^{(m)}[\boldsymbol{i}] \rangle^2 \right)^{1/2}. \tag{5.3}$$

Dunn & Morrison (2003) show a 'dual bi-spectrum' of production, $\mathscr{P}_w + \sigma_{\mathscr{P}}$, at values of $y^+$ lying in the linear sublayer, the buffer region, the log-law region and the outer region; $\sigma_{\mathscr{P}}$ is a measure of the spatial variablility of $\mathscr{P}_w$, and this is largest where the production reaches a maximum, $y^+ \approx 15, k_m\eta \approx 0.07$. Figure 5 shows the flatness of $P^{(m)}[\boldsymbol{i}]$: except for $m = 1$ and 2, it is very large, increasing more or less monotonically as $m$ decreases.

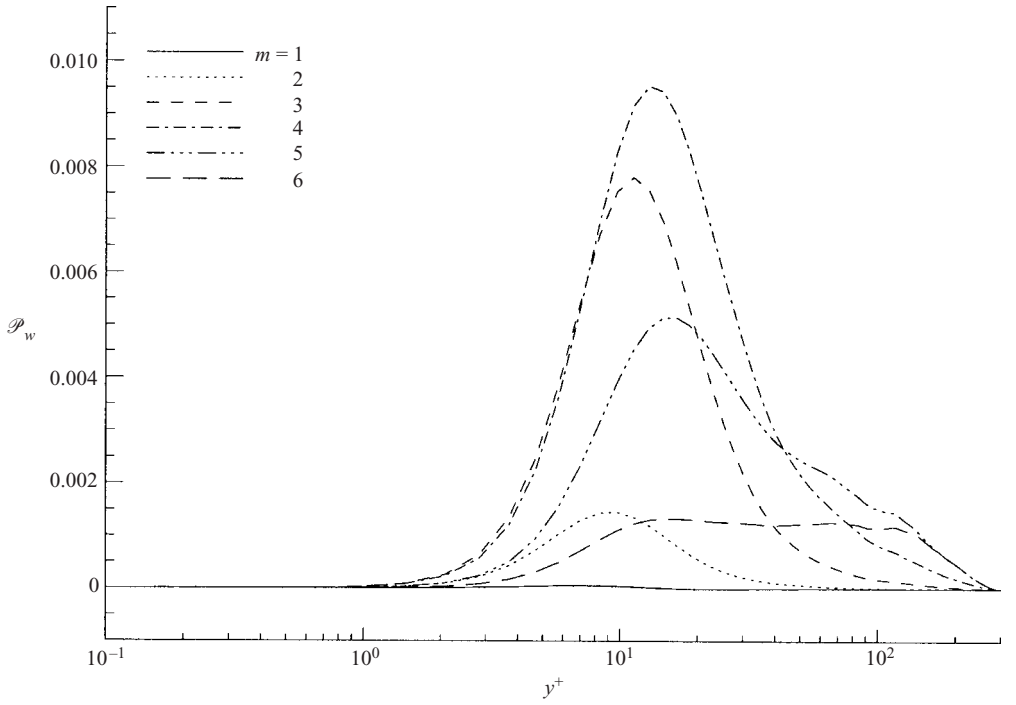


FIGURE 4. Production term, $\mathscr{P}_w(y^+, k_m)$ as a function of $y^+$.

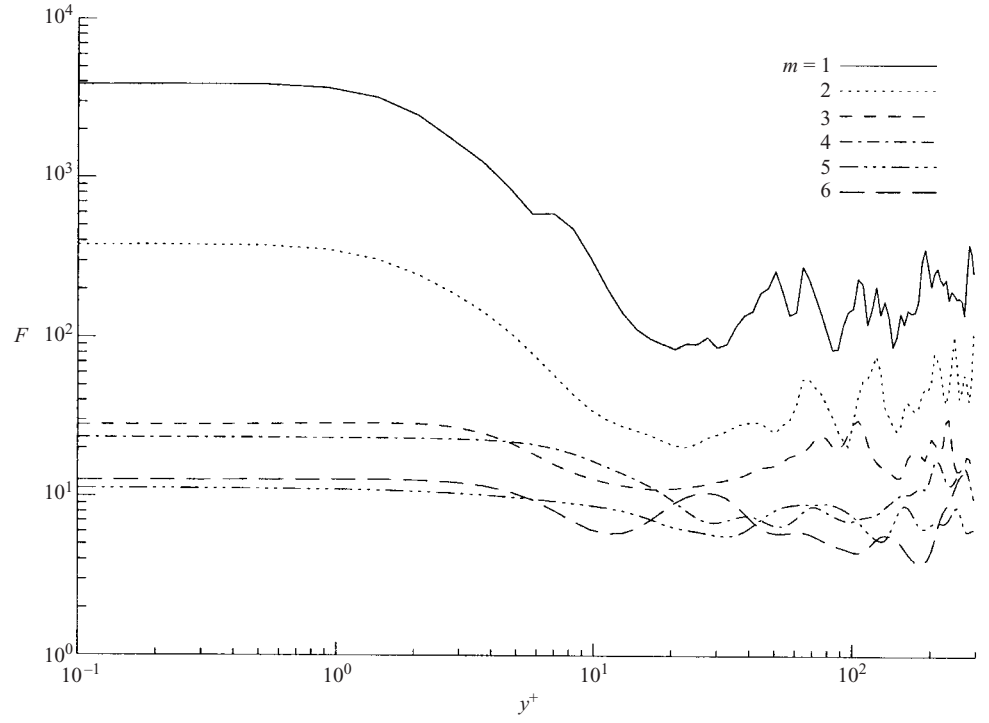


FIGURE 5. Flatness of $P^{(m)}[i]$.

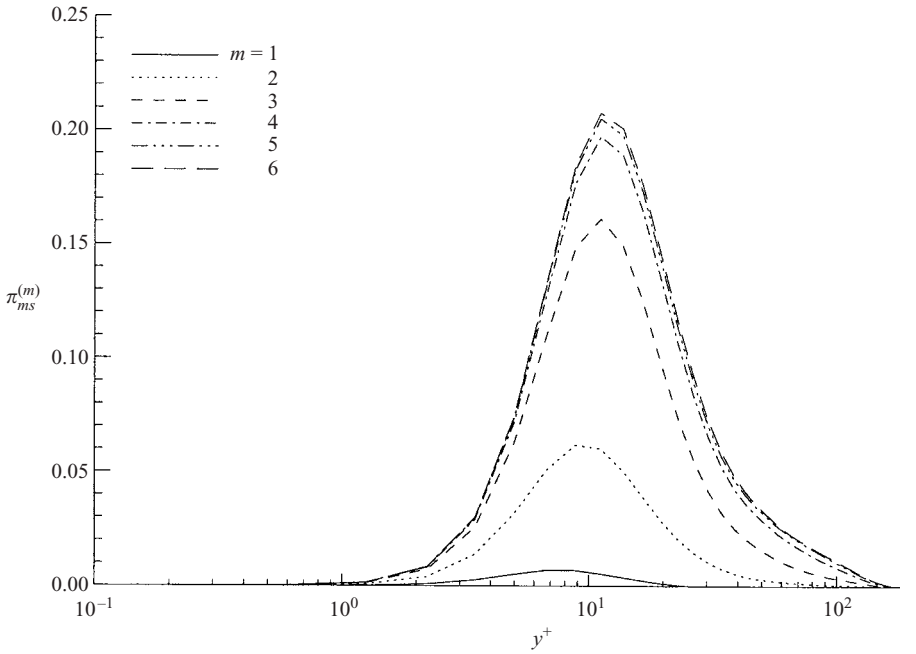


FIGURE 6. $\pi_{ms}^{(m)}$, the production of turbulence kinetic energy in all scales smaller than $r_m$.

Summing $P^{(k)}[\boldsymbol{i}]$ over $k$ for $k = 1, ..., m$ leads to a term

$$\pi_{ms}^{(m)}[\boldsymbol{i}] = \sum_{k=1}^{m} 2^{2(M-k)} P^{(k)}[2^{m-k}\boldsymbol{i}], \tag{5.4}$$

which is the production of turbulence kinetic energy at all scales smaller than $r_m$, i.e. the SGS production. In figure 6, $\pi_{ms}^{(m)}$ increases monotonically with $m$ and the position of the peak is rather less dependent on $m$ than is the case with $P^{(m)}[\boldsymbol{i}]$. Figure 7 shows the flatness of $\pi_{ms}^{(m)}$, a direct analogue of the flatness of $P^{(m)}[\boldsymbol{i}]$, figure 5. Given that calculation of $\pi_{ms}^{(m)}$ involves summation over all modes smaller than $m$, its flatness is very similar to that of $P^{(m)}[\boldsymbol{i}]$ for $m = 1, 2$. At larger $m$ however, the flatness of the former increases tenfold. This implies that the modes are statistically independent.

Figure 8 shows $T^{ms}$, (2.6), which has been calculated using a Fourier cutoff filter, the width of which corresponds to the values of $m$ used for the wavelet filter (table 1). The behaviour of $\pi_{ms}^{(m)}$ is very similar to that of $T^{ms}$, even with regard to the small increase in the value of $y^+$ at which $\pi_{ms}^{(m)}$ reaches a maximum as the filter width increases. Note also that the values of the two quantities are very similar, the differences being attributable only to differences in filter shape.

## 6. Energy flux in wavelet space

Using the SGS stress tensor, a term describing the flux of energy in wavelet space to scales of size $r_m$ from all scales smaller than $r_n$ at position $[\boldsymbol{i}]$ is

$$t^{(m,n)}[\boldsymbol{i}] = -\sum_{i=1}^{3}\sum_{q=1}^{3} w_i^{(m,q)}[\boldsymbol{i}] \left\{ \frac{\partial}{\partial x_j} \tau_{ij}^{(n)} \right\}^{(m,q)} [\boldsymbol{i}]. \tag{6.1}$$

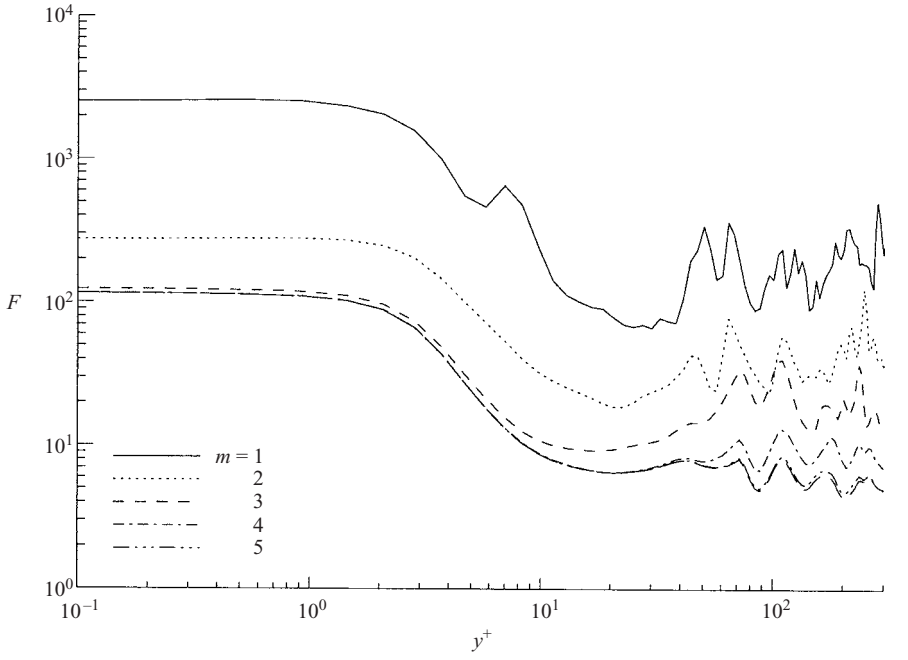


FIGURE 7. Flatness of $\pi_{ms}^{(m)}$.

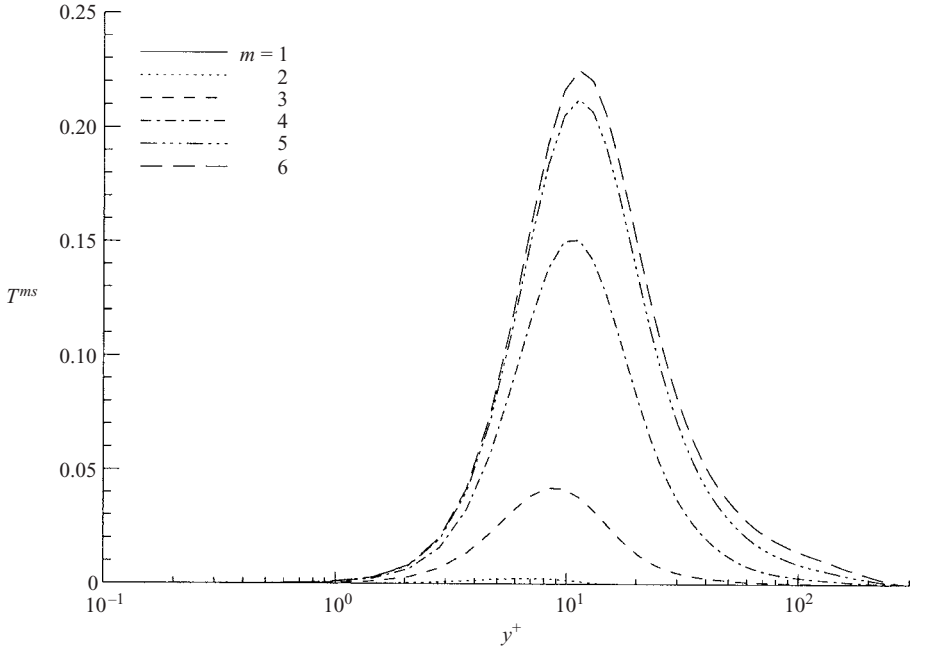


FIGURE 8. Plot of $T^{ms}$, the production of turbulence kinetic energy in the SGS motion, calculated using a Fourier cutoff filter of the same size as the wavelet filter, figure 6.

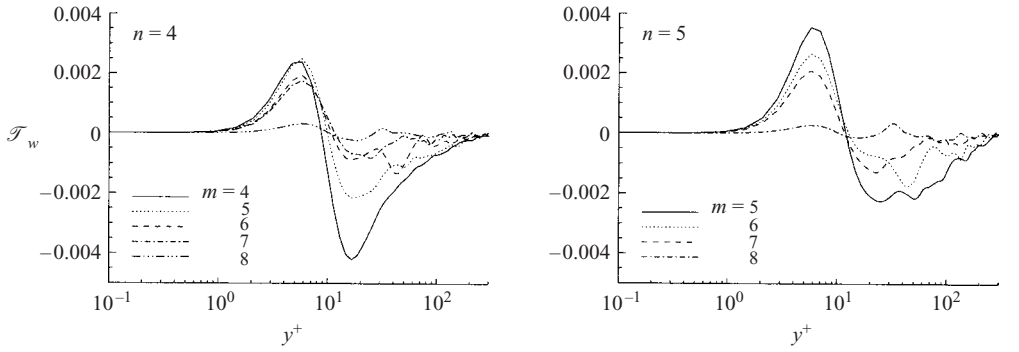


FIGURE 9. Wavelet dual bispectrum of subgrid transfer, $\mathscr{T}_w(y^+, k_m|k_n)$ against $y^+$, for $Re_\tau = 300$.

The sign is negative when backscatter of energy occurs. The corresponding term used by Meneveau (1991) includes the pressure-gradient term which we have chosen to omit here. Flux due to the pressure gradient is addressed separately in the next section. Meneveau (1991) defines a 'dual bi-spectrum of transfer' to scale $r_m$ by interactions with scales smaller than $r_n$, $(n \leqslant m)$, as

$$\mathscr{T}_w(y^+, k_m \,|\, k_n) = \frac{2^{-m}(\Delta_x \Delta_z)^{1/2}}{\pi\sqrt{2}} \langle t^{(m,n)}[\boldsymbol{i}] \rangle, \tag{6.2}$$

the standard deviation of which is

$$\sigma_{m|n} = \frac{2^{-m}(\Delta_x \Delta_z)^{1/2}}{\pi\sqrt{2}} \left( \langle t^{(m,n)}[\boldsymbol{i}]^2 \rangle - \langle t^{(m,n)}[\boldsymbol{i}] \rangle^2 \right)^{1/2}. \tag{6.3}$$

Figure 9 shows $\mathscr{T}_w(y^+, k_m|k_n)$, for $n = 4$ and 5. The flux is numerically largest when $n = m$ and it is therefore local in scale, but the flux both to and from non-adjacent scales is also non-zero on average. In the sublayer, it is predominantly from large to small scales, but note that it is numerically largest when the flux is from the small to the large scales at $y^+ \approx 15$–$20$. This is consistent with the results of Piomelli *et al.* (1996), Härtel & Kleiser (1998) and Domaradzki *et al.* (1994), who have also shown that backscatter is predominant in the buffer region. Dunn & Morrison (2003) show that, for $y^+ \approx 30$, some transfer can be non-local with one leg of the triad close to the viscous cutoff ($n = 1$). Interestingly, the same phenomenon is observed in a plane jet (also at low Reynolds numbers) by Akhavan *et al.* (2000).

Figure 10 shows the dual bi-spectrum of transfer in wavenumber space for $n = 4$, at several values of $y^+$ across the boundary layer. The largest numerical values occur again for $m = n$. The variance is also greatest for $m = n$, but the flux to all 'resolved' scales exhibits both non-zero mean and non-zero variance: the flux can take either sign at different positions in physical space. The greatest spatial variation occurs in the region where the flux has its largest magnitude, $y^+ \approx 15$. The variance of $\mathscr{T}_w(y^+, k_m|k_n)$ is significantly larger than that of any of the quantities in the turbulence kinetic energy budget (see Dunn & Morrison 2003) and it is clear that the mean flux is the small difference between fluxes of large magnitude but of opposite sign. Figure 11 shows the contribution by each velocity component to the flux, i.e. the spectrum (6.1), but with the subscript $i$ fixed. The flux is mainly to (or from) the streamwise component, but the other components exhibit much smaller fluxes which tend to have the same variation with $y^+$ as the streamwise component. Dual

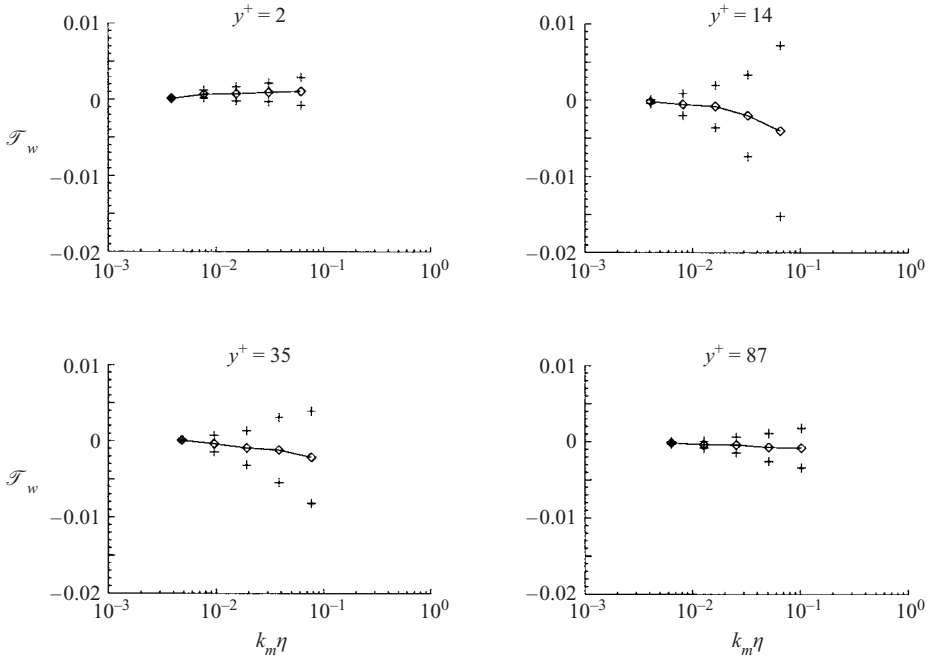


FIGURE 10. Wavelet dual bispectrum of subgrid transfer against $k_m\eta$, $Re_\tau = 300$, $n = 4$.

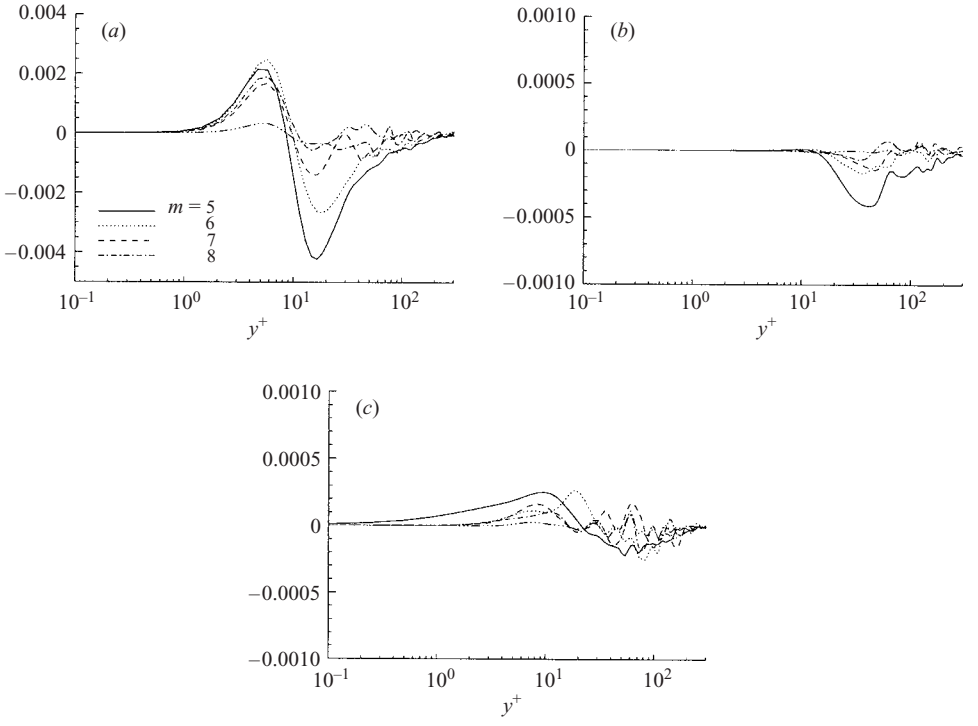


FIGURE 11. Components of $\mathscr{T}_w(y^+, k_m|k_n)$ for $n = 3$: (a) $i = 1$; (b) $i = 2$; (c) $i = 3$.

bi-spectra (not shown) indicate that the variance in the streamwise component is similar to that for the flux term as a whole, while the variances for the spanwise and wall-normal components are much smaller. In summary therefore, the variances of a specific component are large when its mean flux at that wavenumber is large.

The anisotropy of the Reynolds (and subgrid) stresses is usually explained in terms of the change in sign of the wall-normal component of the pressure–strain term at $y^+ \approx 30$ (see, for example, Moin & Kim 1982). The correlation between the pressure and components of the strain rate is responsible for the transfer of energy from the wall-normal stress to the wall-parallel ones. In the case of the components of $\mathscr{T}_w(y^+, k_m \,|\, k_n)$ (figure 11), the explanation requires rather more detail since there appears to be no simple amplification of the wall-parallel components at the expense of the wall-normal one, as a simple 'splatting' argument suggests. Here, the anisotropy arises due to the large wall-normal strain rate, $\partial U/\partial y$, the only component with non-zero mean. Large strain rates are also closely associated with the appearance of quasi-streamwise vortices (see Lee, Kim & Moin 1990), and therefore of large instantaneous pressure gradients in the spanwise and wall-normal directions. The anisotropy of pressure-gradient fluctuations is explored in the next section.

The quantity of most interest for LES modelling is the effective sink (or source) of energy to the subgrid scales. Meneveau (1991) defines the local subgrid flux in wavelet space, by summing the local subgrid transfer over the resolved scales. Specifically, the quantity

$$\pi_{sg}^{(m)}[\boldsymbol{i}] = \sum_{k=m}^{M} 2^{2(M-k)} t^{(k,m)}\left[2^{(m-k)}\boldsymbol{i}\right], \tag{6.4}$$

is the local flux of energy from the resolved-scale motion to the SGS motion, and is positive when the flux is from the resolved scales to the SGS motion (forward scatter) and negative otherwise (backscatter). The interpretation of $\pi_{sg}^{(m)}$ requires some care. In our definition of the subgrid stresses, we have not introduced filtering of the products on the right-hand side of (4.4), as is usually done in LES, (2.2). However, in the definition of $\pi_{sg}^{(m)}$, a summation over all modes above the cutoff is made so that, loosely speaking, summation of a band-passed wavelet flux at each mode is qualitatively equivalent to the low-pass filtering of conventional filters such as the sharp Fourier cutoff. However, since the orthogonal wavelet filtering operation does not commute with differentiation, it is not possible to split $\pi_{sg}^{(m)}$ into two terms, one representing SGS diffusion, the other SGS dissipation (the transfer between resolved and subgrid scales). Hence, $\pi_{sg}^{(m)}$ contains spatial flux, which cannot be separated from the true SGS dissipation. However, note that in calculating $\pi_{sg}^{(m)}$ only the fluctuating velocity components have been used, i.e. production due to the mean strain rate is not included. Therefore, $\pi_{sg}^{(m)}$ is analogous to $\epsilon_{sg}$, (2.3), but calculated using only the fluctuating velocity components. Alternatively, $\pi_{sg}^{(m)}$ is equivalent to the term $T^{fs}$ of (2.6*b*), but with an additional component of SGS diffusion. The spectra of subgrid flux,

$$\pi_{sg}(y^+, k_m) = 2^{-2m}\left\langle \pi_{sg}^{(m)}[\boldsymbol{i}]\right\rangle, \tag{6.5}$$

are plotted in figure 12. For $m = 1$, lying close to the viscous cutoff, the flux is small and positive across the whole channel, in keeping with the conventional energy cascade. For $m = 3$, 4 and 5, lying in the $-5/3$ region of the energy spectra, the subgrid flux is largest in magnitude. In the linear sublayer, it is positive for all scales, indicating that energy flux is to smaller scales, consistent with an unsteady, linear, Couette-like vortex stretching. At larger $y^+$, the flux becomes dominated by nonlinear

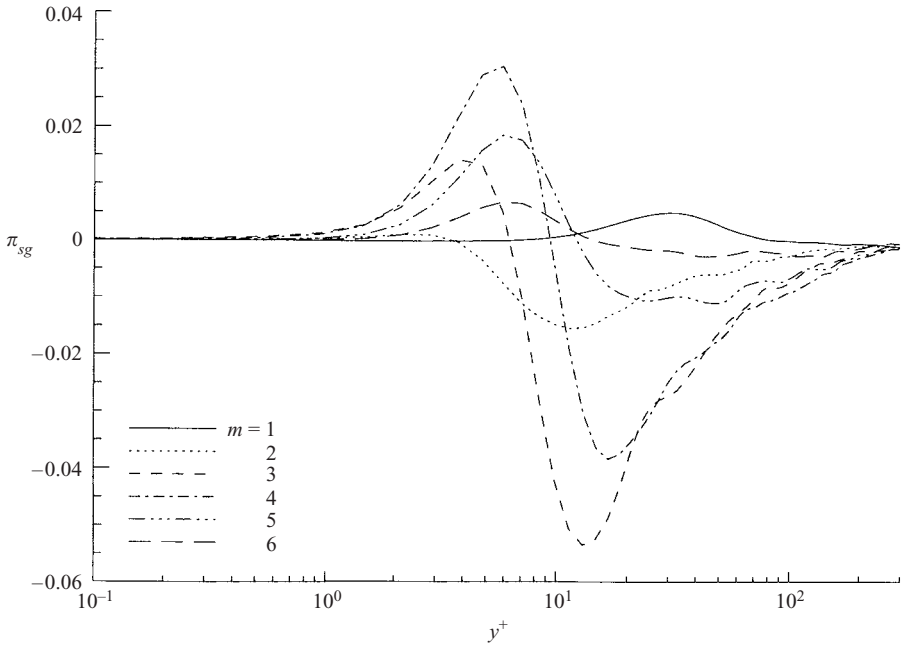


FIGURE 12. Subgrid flux, $\pi_{sg}(y^+, k_m)$ for $Re_\tau = 300$.

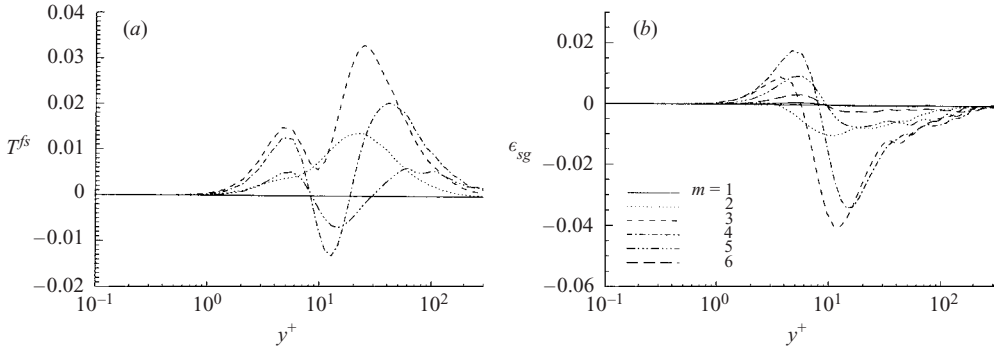


FIGURE 13. (*a*) $T^{fs}$ and (*b*) $\epsilon_{sgs}$ against $y^+$. The values of $m$ in the legend refer to use of a cutoff filter with the same width as the wavelet scale, $r_m$.

processes, and is large and negative across the buffer region. Backscatter is most significant in the region of maximum production ($y^+ \approx 15$).

For comparison, figure 13 shows $T^{fs}$ and $\epsilon_{sg}$, evaluated using a Fourier cutoff filter of the same width as the wavelet modes. It is apparent that $\epsilon_{sg}$ is very similar to $\pi_{sg}^{(m)}$, exhibiting a positive peak in the sublayer and a larger negative peak in the buffer region. These peaks are, in fact, slightly smaller than the equivalent ones for $\pi_{sg}^{(m)}$ because of the effects of the single-signed mean strain rate. On the other hand, $T^{fs}$ (figure 13*a*) shows a region of backscatter only for $m = 4$ and 5. This is because a Fourier cutoff filter operation operates over all space and so is immune to large spatial variations in energy flux evident in the equivalent wavelet terms.

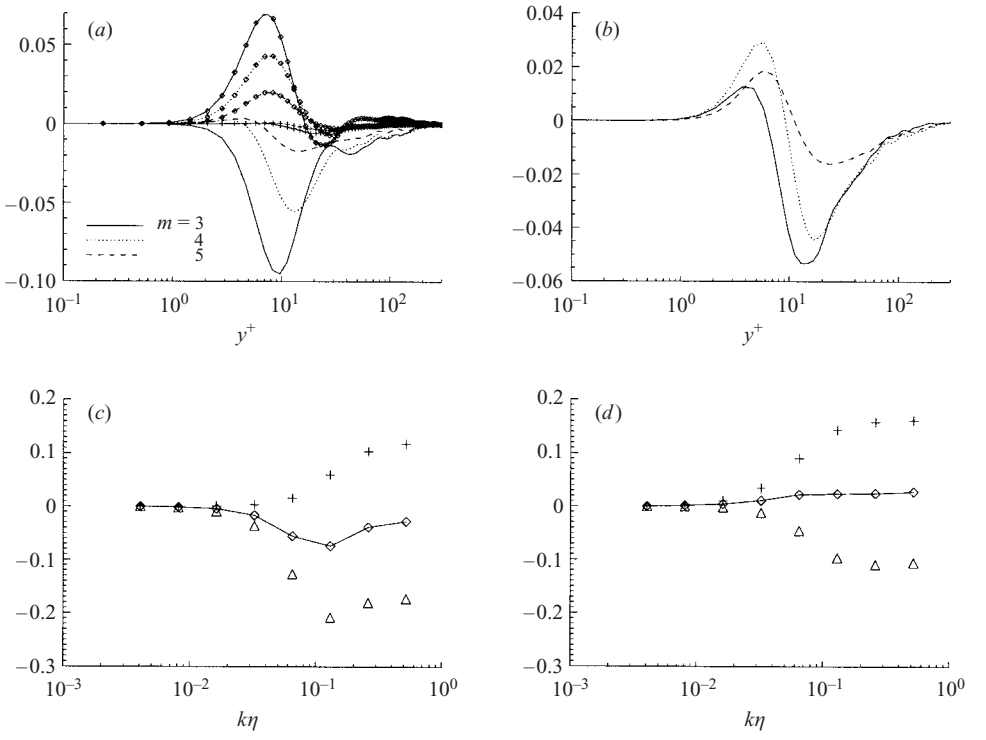


FIGURE 14. Anisotropy of the SGS flux. (*a*) Plane-averages of $\pi^{(m)}_{sg,12}$ (no symbols); $\pi^{(m)}_{sg,13}$ (diamonds) and $\pi^{(m)}_{sg,11}$ (crosses). (*b*) Plane-average of the sum $\pi^{(m)}_{sg,11}+\pi^{(m)}_{sg,12}+\pi^{(m)}_{sg,13}$. The bottom two plots are dual bispectra of SGS flux components: (*c*) $\pi^{(m)}_{sg,12}$ and (*d*) $\pi^{(m)}_{sg,13}$, both evaluated at $y^+ \approx 16$.

To investigate the effects of anisotropy further, we consider

$$\pi^{(m)}_{sg,ij}[\boldsymbol{i}] = \sum_{k=m}^{M} 2^{2(M-k)} t^{(k,m)}_{ij}\left[2^{(m-k)}\boldsymbol{i}\right], \tag{6.6}$$

where

$$t^{(m,n)}_{ij}[\boldsymbol{i}] = -\sum_{i=1}^{3}\sum_{q=1}^{3} w^{(m,q)}_{i}[\boldsymbol{i}]\left\{\frac{\partial}{\partial x_j}\tau^{(n)}_{ij}\right\}^{(m,q)}[\boldsymbol{i}], \tag{6.7}$$

and no summation on $i$ and $j$ is implied – that is $\pi^{(m)}_{sg,ij}$ is the flux due only to the $ij$ component of the SGS stress tensor. Figure 14(*a*) shows the components of $\pi^{(m)}_{sg,ij}$ which include the streamwise velocity component (i.e. $ij = 11,\ 12$ and 13). Figure 14(*b*) shows the sum of these components for each $m$. Comparison with figure 12 shows that most of the mean SGS flux involves SGS stresses that include streamwise momentum. Moreover, the component that is aligned with the largest component of the resolved strain-rate tensor ($ij = 12$) is large and negative in the mean. The component containing spanwise momentum, corresponding to a zero-mean component of the resolved strain-rate tensor ($ij = 13$), is large and positive. The remaining component ($ij = 11$) involves the streamwise SGS kinetic energy, the largest component of the SGS stresses, but has a very small mean contribution to the SGS flux. The components not shown exhibit negligible mean values.

Figures 14(*c*) and 14(*d*) show dual bispectra of $\pi^{(m)}_{sg,12}$ and $\pi^{(m)}_{sg,13}$, calculated at $y^+ \approx 16$. The standard deviation is greatest for scales near the viscous cutoff and in the $-5/3$ spectral region. It is of similar magnitude in the sublayer and decreases towards the centre of the channel (not shown). Therefore it is clear that both components of the SGS flux can take either sign locally. The standard deviation of these two components is the largest of all nine and is about twice that of $\pi^{(m)}_{sg,11}$. The spatial variability of the other six components is typically an order of magnitude less, even though they all have standard deviations which, as multiples of mean, are as large as those for components in which the spatial variability is the largest. An important feature of figure 14(*c*, *d*) is the large spatial variability even in the scales near the viscous cutoff when $\pi^{(m)}_{sg,12}$ and $\pi^{(m)}_{sg,13}$ are small. This is in contrast to other wavelet quantities such as $\mathscr{P}^{(m)}$, $\mathscr{V}^{(m)}$ and the other components of $\pi^{(m)}_{sg}$ and first appears in the transfer term, $\mathscr{T}_w(y^+, k_n|k_m)$. This indicates that the spatial intermittency appears largely in those components of the nonlinear inertial flux term, $\pi^{(m)}_{sg}$, that contain the gradients of SGS stress components, $\partial\tau_{12}/\partial y$ and $\partial\tau_{13}/\partial z$.

## 7. The pressure-gradient term

We now turn our attention to subgrid flux effected by the pressure-gradient term in the Navier–Stokes equations,

$$\pi^{(m)}_{sg,p}[\boldsymbol{i}] = \sum_{k=m}^{M} 2^{2(M-k)} t_p^{(k,m)}\left[2^{(m-k)}\boldsymbol{i}\right], \tag{7.1}$$

where

$$t_p^{(m,n)}[\boldsymbol{i}] = -\sum_{i=1}^{3}\sum_{q=1}^{3} w_i^{(m,q)}[\boldsymbol{i}]\left\{\frac{1}{\rho}\frac{\partial p^{<n}}{\partial x_i}\right\}^{(m,q)}[\boldsymbol{i}], \tag{7.2}$$

which has so far been neglected. Note that $t_p^{(m,n)}$ relates to the small-scale pressure field as it is the result of the same high-pass filtering operation already applied to the velocity field in §4. Dunn & Morrison (2003) provide further details. Figure 15 shows that $\pi^{(m)}_{sg,p}$ is about two orders of magnitude smaller than $\pi^{(m)}_{sg}$, and is, in fact, comparable to $\pi^{(m)}_{sg,ij}$ for $ij \neq 12$ or 13. This supports the neglect of energy transfer by the pressure gradient in almost all subgrid models and filters. Note that when $n = 8$ in (7.2), and $\pi^{(m)}_{sg,p}$ is summed over all $m$, the velocity/pressure-gradient term appearing in the conventional energy balance, $\Pi_{kk}$, is recovered (see Mansour *et al.* 1988).

More physically, Kim (1989) shows that, in channel flow at $Re_\tau = 179$, the static pressure is only slightly negatively skewed, but has flatness factors that are typically twice the Gaussian value of 3 over much of the channel height. Batchelor & Townsend (1956) have suggested that, at Reynolds numbers high enough for local isotropy, the mean-square pressure gradient is much larger than the mean-square viscous force,

$$\frac{1}{\rho^2}\overline{\left(\frac{\partial p}{\partial x_i}\right)^2} \approx 20\nu^2\overline{\left(\frac{\partial^2 u_i}{\partial x_j^2}\right)^2}, \tag{7.3}$$

in which the term involving viscous diffusion is ignored. Figure 16 shows that, outside the viscous sublayer, the factor of 20 is about right, even at low Reynolds numbers. Equation (7.3) suggests that the mean-square acceleration comprises prolonged viscous intervals 'pulsed' periodically by the mean-square pressure gradient. Thus a pressure

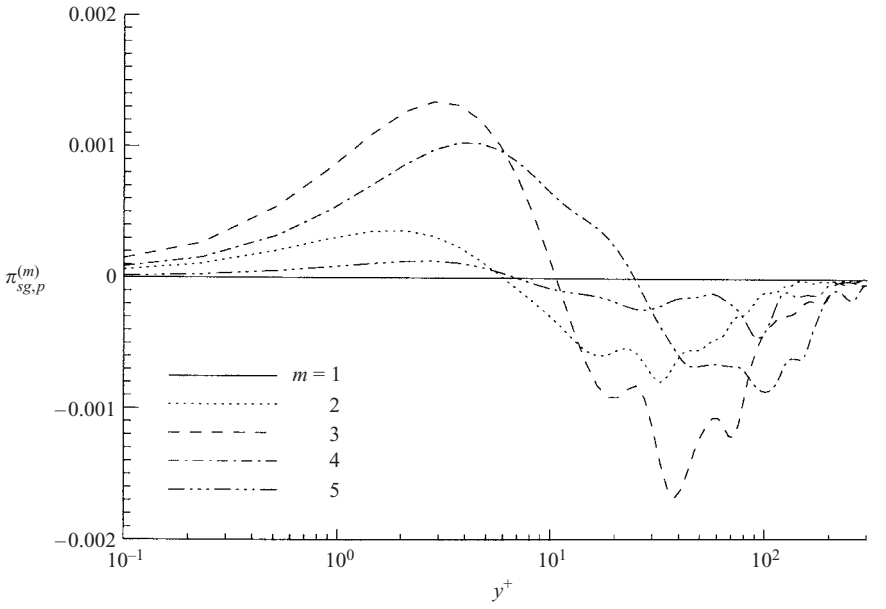


FIGURE 15. Plane-averages of $\pi^{(m)}_{sg,p}$ as a function of $y^+$.

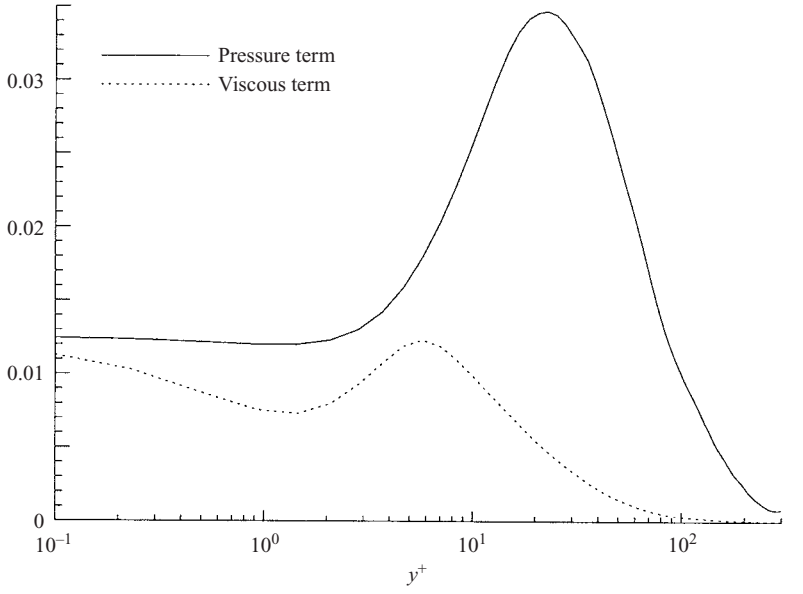


FIGURE 16. Mean-square pressure gradient and mean-square viscous force, defined by (7.3).

field of small skewness, but large flatness, gives rise to a pressure-gradient distribution of which the first moment is very small, but of which even moments are significantly larger. Kim (1989) also shows that contributions to the mean-square wall pressure are principally local in nature even though the instantaneous wall pressure receives significant contributions from the opposite wall. Therefore, the mean-square pressure close to the surface is intimately related to the structure there. In terms of the sublayer populated with quasi-streamwise vortices, this means merely that a low-pressure

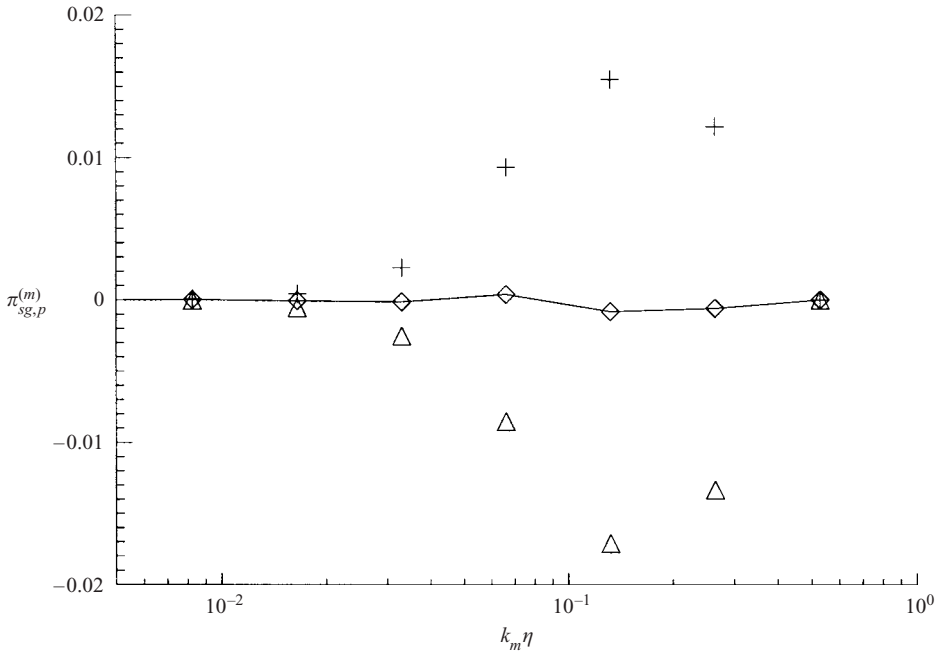


FIGURE 17. $\pi^{(m)}_{sg,p}$ as a function of $k_m\eta$, evaluated at $y^+ \approx 16$.

region (approximately coinciding with the vortex core) always has two opposite-signed pressure gradients in the cross-sectional plane of the vortex. The present data show that, at $y^+ \approx 25$, $\overline{(\partial p/\partial x)^2} \approx 0.5\overline{(\partial p/\partial y)^2} \approx 0.5\overline{(\partial p/\partial z)^2}$. Kim (1989) also notes that $\partial p/\partial x$ is not a good indicator of quasi-streamwise vortices while vertical and spanwise gradients are.

Statistically, this means that quantities such as $\pi^{(m)}_{sg,p}$ involving the first moment of pressure-gradient fluctuations are small. This is true of the individual components of $\pi^{(m)}_{sg,p,i}$ (not shown). Mansour *et al.* (1988) show that $\Pi_{11} \approx \Pi_{22} + \Pi_{33}$ and $\pi^{(m)}_{sg,p,1} \approx \pi^{(m)}_{sg,p,2} + \pi^{(m)}_{sg,p,3}$ too. While the spanwise component makes the largest (positive) contribution in the linear sublayer, the streamwise component makes the largest (negative) contribution near $y^+ \approx 25$. This means that the component terms, $\pi^{(m)}_{sg,p,i}$, are not much larger than $\pi^{(m)}_{sg,p}$ itself.

In contrast, quantities involving even moments are large, so that the mean-square pressure gradient contributes nearly all of the mean-square acceleration even in the viscous sublayer where it reaches a maximum at $y^+ \approx 25$. This is just the region in which the spatial variability (the root-mean-square) of $\pi^{(m)}_{sg,p}$ and all the components of $\pi^{(m)}_{sg}$ are greatest. In terms of SGS modelling, pressure fluctuations which reside mostly in the large scales effect negligible local transfer of energy between the resolved and subgrid scales. Similarly, pressure-gradient fluctuations which reside predominantly in the small scales do not contribute to energy flux either. On the other hand, the mean-square pressure gradient makes the dominant contribution to the mean-square acceleration, and therefore pressure-gradient fluctuations contribute directly to the spatial intermittency of energy flux even when, on average, some of its components are small.

Figure 17 shows the spatial variability of $\pi^{(m)}_{sg,p}$. It is similar to that for the components of $\pi^{(m)}_{sg,ij}$, $ij \neq 12$ or 13, in that it falls sharply towards the viscous cutoff. By

comparison, the components $\pi^{(m)}_{sg,ij}$, $ij = 12$ or 13 do not (figures 14*a* and 14*b*). In fact, the largest spatial variability of $\pi^{(m)}_{sg,p}$ tends to occur at wavenumbers only slightly higher than those at which the two-dimensional energy spectra reach a maximum (Dunn & Morrison 2003). Kim (1989) shows that pressure fluctuations are well-correlated across the channel height and one might therefore speculate that pressure fluctuations in the outer region, carried by the large scales, also have an important role nearer the wall. Holmes, Lumley & Berkooz (1996) have suggested that outer-region pressure fluctuations trigger the bursting process.

## 8. Discussion and conclusions

The wavelet transform has been used to study energy flux in turbulent channel flow in a manner that is similar to the usual *a priori* testing via conventional real-space or Fourier-space filters. This has enabled mixed spatial and scale-to-scale statistics to be constructed, offering a compromise between a spatial description (e.g. Härtel & Kleiser 1998; Härtel *et al.* 1994; Piomelli *et al.* 1996) and a Fourier description (Domaradzki *et al.* 1994). The orthogonal wavelet transform of Mallat (1989) used here gives the best compromise between resolution in real space and wavenumber space (Meneveau 1991). By paying particular attention to production in the subgrid scales and dissipation in the resolved scales, we have been able to make a detailed study of energy flux. Since the orthogonal wavelet transform does not commute with differentiation, it has not been possible to construct precise analogues of all conventional LES quantities. In order to show relevance to current LES practice, we have compared the wavelet-transformed quantities with equivalent quantities computed using the Fourier cutoff filter. A particular advantage of the mixed space-scale description of energy flux is that its spatial variability has been highlighted.

Particular attention has been paid to low-Reynolds-number effects in the form of production in the SGS motion, and direct viscous dissipation in the GS motion. Following Härtel & Kleiser (1998), we have generated an equivalent wavelet quantity, $\pi^{(m)}_{ms}$, similar to $T^{ms}$ calculated using a sharp Fourier cutoff. The maximum spatial variation of production, $P^{(m)}$, occurs for $y^+ \approx 15$ and for wavenumbers lying in the $-5/3$ region of the velocity spectra. While the skewness of $P^{(m)}$ is not particularly large, its flatness at these locations is as much as 30. Production is therefore highly intermittent and, in an Eulerian frame, occurs in localized, intense bursts. Dunn & Morrison (2003) have shown that the wavelet-transformed viscous term shows similar effects.

The maximum value of $R_\lambda$ for the present data set is about 100, but is strongly dependent on $y^+$. Figure 18 shows the ratio $\pi^{(m)}_{sg}/\mathscr{P}_w$ which has magnitudes (of either sign) close to 9 and 7 for $y^+ \approx 5$ and 15 respectively, for modes in the $-5/3$ range. Thus in the present context, an equivalent criterion to Bradshaw's ($R_\lambda > 100$) for the existence of a first-order subrange is $\pi^{(m)}_{sg}/\mathscr{P}_w > 10$. This is very much within the spirit of his suggestion that sources or sinks are a small fraction of the spectral transfer. Since local isotropy could not be considered a reasonable approximation so close to the wall under any circumstance, such a definition is a more appropriate one for LES of wall-bounded flows.

Using the wavelet-based filter, the term $t^{(m,n)}$, representing the flux of energy between scales of size $r_m$ and all scales smaller than $r_n$, has been calculated. This term is unique to the wavelet representation: a Fourier cutoff filter simply yields the bulk transfer between the resolved scales and the SGS motion, without reference to which of the resolved scales are involved. Analysis of $t^{(m,n)}$ reveals that the transfer is

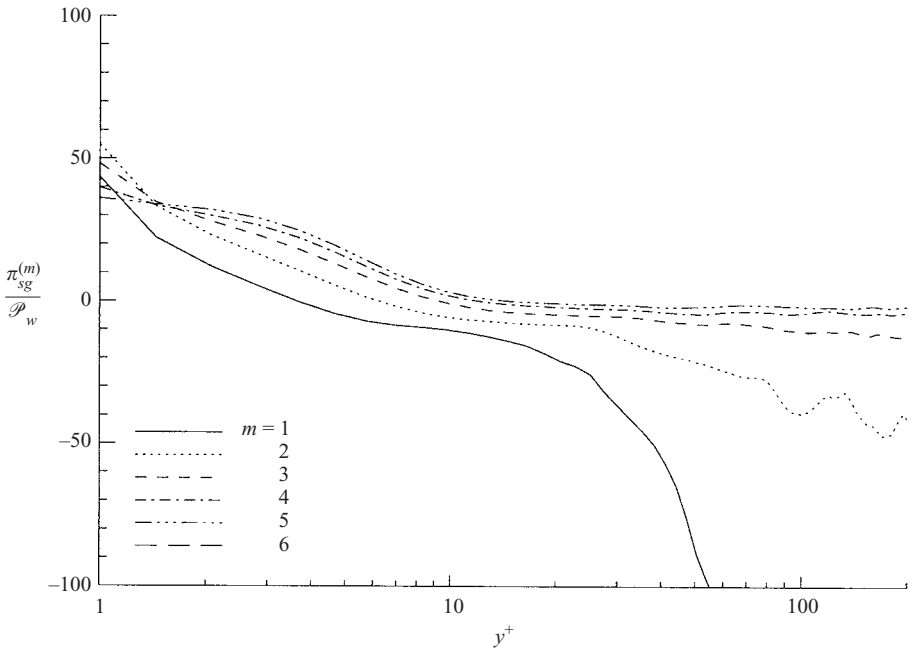


FIGURE 18. The ratio $\pi_{sg}^{(m)}/\mathscr{P}_w$.

predominantly local, in keeping with Kolmogorov (1941) phenomenology. The details are more complicated however. Energy can be transferred between the SGS motion and any of the resolved scales. As in the case of $P^{(m)}$, the variance of $t^{(m,n)}$ is largest when $n$ corresponds to a scale in the $-5/3$ range. The flux can take either sign locally, but is predominantly negative (backscatter) for $y^+ \approx 15$, in agreement with the results of Härtel & Kleiser (1998), Piomelli *et al.* (1996) and others.

Assuming that the spatial variability observed is closely related to the appearance of coherent structures, in this case quasi-streamwise vortices, and that, by definition, these structures are persistent, then it is very likely that intermittency manifests itself not only spatially, but also temporally. Härtel & Kleiser (1998) indicate that the time derivative of the '13' component of the SGS stress is dominant. Figure 19 shows the correlation of $\pi_{sg}^{(m)}$ with streamwise and spanwise separations for $m = 1$. The loss of spatial resolution when using the wavelet transform limits the usefulness of correlations for large values of $m$. While the SGS flux has a correlation lengthscale of about 200 wall units in the streamwise direction, it is only about 50 wall units in the spanwise direction. A clear physical picture emerges based on a quasi-streamwise vortex. Its stretching and rotation leads to local scale-to-scale energy transfer while its circulation leads to lateral and wall-normal transport of streamwise momentum.

A particular difficulty arises in attempting to condition $\pi_{sg}^{(m)}$ based on the appearance of ejections or sweeps: while the latter are defined with respect to the DNS grid, the former are sparsely defined in the larger modes. In future work, we propose to use undecimated wavelets so that by retaining some redundancy, quantities such as $\pi_{sg}^{(m)}$ may be specified at every DNS mesh point. An approximate idea of the suggested relationship between ejections, sweeps and spectral flux may be gained by using $T^{fs}$. Figure 20 shows contributions made by ejections ($uv_2$) and sweeps ($uv_4$) to $T^{fs}$. Here, ensemble averages of $T^{fs}$ are made using points for which $uv > var(uv)$, where $var(uv)$ is the local variance of the $uv$-signature. $T^{fs}$ is calculated with a cutoff in the

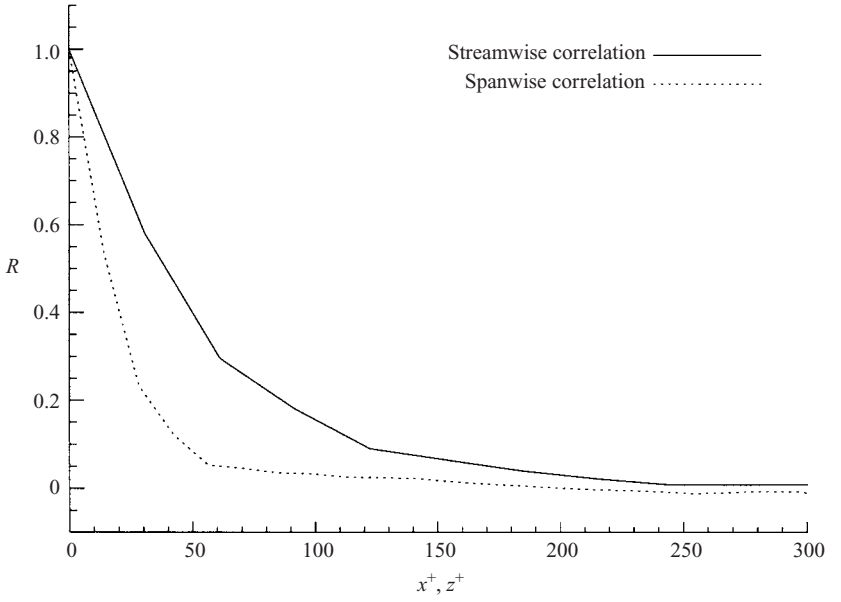


FIGURE 19. The streamwise and spanwise correlation functions of $\pi_{sg}^{(m)}$ for $m = 1$.

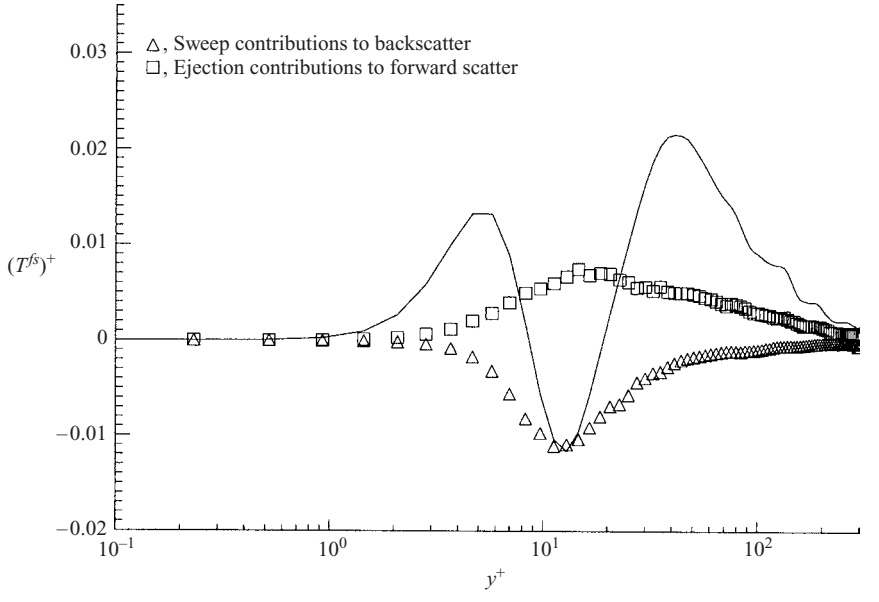


FIGURE 20. Contributions by ejections and sweeps to $T_{fs}$.

−5/3 spectral region. Although the results are dependent on the sampling used and the filter size, they do show that sweeps are significant contributors to backscatter in the sublayer. Clearly a wavelet representation would be much more revealing.

It is highly likely that the anisotropy of the Reynolds stresses and the subgrid stresses is not limited to wall flows, but applies to any flow with large-scale anisotropy. In the Fourier transformed Navier–Stokes equations, the nonlinear term couples the motion at any particular wavenumber with all other wavenumbers. Brasseur & Wei

(1994) have shown that distant triadic interactions tend to transmit any large-scale anisotropy down to the smallest scales of the flow. In the context of wall turbulence, the pressure is important in this respect. Anisotropy also appears in $\pi_{sg}^{(m)}$, the SGS flux term that is analogous to $\epsilon_{sg}$ in LES modelling. The SGS flux involving the '12' component of the SGS stress tensor, and so aligned with the mean strain rate, is the largest in magnitude and is responsible for backscatter across the wall region. The SGS flux involving the '13' component of the SGS stress tensor is responsible for the forward scatter near the wall. Note that in this case, the corresponding strain rate of the resolved scales has a zero mean value. Both 12 and 13 components are unique in that they exhibit large spatial variability down to the viscous cutoff. This is consistent with the suggested importance of quasi-streamwise vortices to energy flux. The other components of the SGS stress tensor do not contribute significantly to the SGS flux in the mean.

The energy flux due to the pressure-gradient term has been shown to be negligibly small and the component terms are also. The importance of the pressure gradients lies in their even moments and the second moment contributes nearly all of the mean-square acceleration. While spatial variability is apparent in all the wavelet-transformed quantities irrespective of direction, it is considerably larger (by a factor of 5 or 6) for quantities involving the nonlinear term. Because the standard deviation as a multiple of the mean is large for all components of the flux, and it occurs in the wavenumber range in which it is expected that the spectrum of pressure-gradient fluctuations reaches a maximum (equivalent to the $-5/3$ range of the velocity spectra), spatial variability may be explained as a consequence of the dominant contribution made by the mean-square pressure gradient to the mean-square acceleration.

The present results appear to be consistent with the suggestion by Akhavan *et al.* (2000) that structure is the cause of spatial variability and that therefore detailed behaviour of flux is unlikely to be captured by eddy viscosity models. This is certainly the case for local fluxes. Dunn & Morrison (2003) show that there is also non-local flux, which although small, is always positive and therefore appropriately modelled by eddy viscosity models.

We are indebted to Philippa Westbury who undertook much early work and to Neil Sandham of the University of Southampton for access to the DNS data generated as part of the efforts of the UK Turbulence consortium (EPSRC GR/M08424, GR/R26368 & GR/R64957). We are indebted to Charles Meneveau for helpful correspondence. We acknowledge financial support from EPSRC (GR/M31187).

## REFERENCES

Akhavan, R., Ansari, A., Kang, S. & Mangiavacchi, N. 2000 Subgrid-scale interactions in a numerically simulated planar jet and implications for modelling. *J. Fluid Mech.* **408**, 83–120.

Batchelor, G. K. & Townsend, A. A. 1956 Turbulent diffusion. In *Surveys in Mechanics* (ed. G. K. Batchelor & R. M. Davies), pp. 352–399. Cambridge University Press.

Bradshaw, P. 1967 Conditions for the existence of an inertial subrange in turbulent flow. *Natl Phys. Lab. Aero. Rep.* 1220.

Brasseur, J. G. & Wei, C.-H. 1994 Interscale dynamics and local isotropy in high reynolds number turbulence with triadic interactions. *Phys. Fluids* **6**, 842–870.

Do-Khac, M., Basdevant, C., Perrier, V. & Dang-Tran, K. 1994 Wavelet analysis of 2D turbulent fields. *Physica* D **76**, 252–277.

Domaradzki, J., Liu, W., Härtel, C. & Kleiser, L. 1994 Energy transfer in numerically simulated wall-bounded turbulent flows. *Phys. Fluids* **6**, 1583–1599.

Dunn, D. C. & Morrison, J. F. 2000*a* Analysis of coherent structures in turbulent channel flow using the orthogonal wavelet representation. In *Advances in Turbulence VIII* (ed. C. Dopazo), pp. 671–674. CIMNE Barcelona.

Dunn, D. C. & Morrison, J. F. 2000*b* Energy transfers in wall turbulence. *IC Aero Rep*. 00-01. Department of Aeronautics, Imperial College.

Dunn, D. C. & Morrison, J. F. 2001 Energy flux in turbulent channel flow using orthogonal wavelets. *IC Aero Rep*. 01-06. Department of Aeronautics, Imperial College.

Dunn, D. C. & Morrison, J. F. 2003 Analysis of the energy budget in turbulent channel flow using orthogonal wavelets. *Computers Fluids* (submitted).

Durbin, P. & Speziale, C. G. 1991 Local anisotropy in strained turbulence at high reynolds numbers. *Trans. ASME: J. Fluids Engng* **113**, 707–709.

Farge, M. 1989 Wavelet transforms and their application to turbulence. *Annu. Rev. Fluid Mech.* **24**, 395–457.

Ferziger, J. H. & Perić, M. 1996 *Computational Methods for Fluid Dynamics*. Springer.

Germano, M., Piomelli, U., Moin, P. & Cabot, W. H. 1991 A dynamic subgrid-scale eddy viscosity model. *Phys. Fluids* A **3**, 1760–1765.

Härtel, C. & Kleiser, L. 1997 Galilean invariance and filtering dependence of near-wall grid-scale/subgrid-scale interactions in large-eddy simulation. *Phys. Fluids* **9**, 473–475.

Härtel, C. & Kleiser, L. 1998 Analysis and modelling of subgrid-scale motions in near-wall turbulence. *J. Fluid Mech.* **356**, 327–352.

Härtel, C., Kleiser, L., Unger, F. & Friedrich, R. 1994 Subgrid-scale energy transfer in the near-wall region of turbulent flows. *Phys. Fluids* **6**, 3130–3143.

Holmes, P., Lumley, J. L. & Berkooz, G. 1996 *Turbulence, Soherent Structures, Dynamical Systems and Symmetry*. Cambridge University Press.

Kim, J. 1989 On the structure of pressure fluctuations in simulated turbulent channel flow. *J. Fluid Mech.* **205**, 421–451.

Kolmogorov, A. N. 1941 The local structure of turbulence in incompressible viscous fluids for very large reynolds numbers. *C. R. Akad. Sci. SSSR* **30**, 301–305.

Lee, M. J., Kim, J. & Moin, P. 1990 Structure of turbulence at high shear rate. *J. Fluid Mech.* **216**, 561–583.

Leonard, A. 1974 Energy cascade in large-eddy simulation of turbulent fluid flow. *Adv. Geophys.* A **18**, 237–248.

Lund, T. S. 1997 On the use of discrete filters for large eddy simulations. *Center for Turbulence Research Annual Research Briefs*. Stanford University.

Mallat, S. G. 1989 A theory for multireslution signal decomposition: the wavelet representation. *IEEE Patt. Anal. Mach. Intl* **11**, 674–693.

Mansour, N. N., Kim, J. & Moin, P. 1988 Reynolds-stress and dissipation rate budgets in a turbulent channel flow. *J. Fluid Mech.* **194**, 15–44.

Mason, P. J. & Thomson, D. J. 1992 Stochastic backscatter in the large-eddy simulations of boundary layers. *J. Fluid Mech.* **242**, 51–78.

Meneveau, C. 1991 Analysis of turbulence in the orthonormal wavelet representation. *J. Fluid Mech.* **232**, 469–520.

Meneveau, C. 1994 Statistics of turbulence subgrid-scale stresses: Necessary conditions and experimental tests. *Phys. Fluids* **6**, 815–833.

Moin, P. & Kim, J. 1982 Numerical investigation of turbulent channel flow. *J. Fluid Mech.* **118**, 341–377.

Morrison, J. F., Jiang, W., McKeon, B. J. & Smits, A. J. 2002*a* Reynolds-number dependence of streamwise velocity fluctuations in turbulent pipe flow. *AIAA Paper* 2002-0574.

Morrison, J. F., Jiang, W., McKeon, B. J. & Smits, A. J. 2002*b* Reynolds-number dependence of streamwise velocity spectra in turbulent pipe flow. *Phys. Rev. Lett.* **88**, 214501.

Morrison, J. F., Subramanian, C. S. & Bradshaw, P. 1992 Bursts and the law of the wall in turbulent boundary layers. *J. Fluid Mech.* **241**, 75–108.

Murray, J. A., Piomelli, U. & Wallace, J. M. 1996 Spatial and temporal filtering of experimental data for *a priori* studies of subgrid stresses. *Phys. Fluids* **8**, 1978–1980.

Nicoud, F., Baggett, J. S., Moin, P. & Cabot, W. 2001 Large eddy simulation wall-modeling based on suboptimal theory and linear stochastic estimation. *Phys. Fluids* **13**, 2968–2984.

Piomelli, U. & Balaras, E. 2002 Wall-layer models for large-eddy simulations. *Annu. Rev. Fluid Mech.* **34**, 349–374.

Piomelli, U., Yu, Y. & Adrian, R. J. 1996 Subgrid-scale energy transfer and near-wall turbulence structure. *Phys. Fluids* **8**, 215–224.

Porté-Agel, F., Meneveau, C. & Parlange, M. C. 2000 A scale-dependent dynamic model for large-eddy simulation: application to a neutral atmospheric boundary layer. *J. Fluid Mech.* **415**, 261–284.

Qiu, J., Paw, U. K. T. & Shaw, R. H. 1995 The leakage problem of orthonormal wavelet transforms when applied to atmospheric turbulence. *J. Geophys. Res.* **100**, 25,769–25,779.

Redelsperger, J. L., Mahé, F. & Carlotti, P. 2001 A simple and general subgrid model suitable both for surface layer and free-stream turbulence. *Boundary-Layer Met.* **101**, 375–408.

Robinson, S. K. 1991 Coherent motions in the turbulent boundary layer. *Annu. Rev. Fluid Mech.* **23**, 601–639.

Saddoughi, S. G. & Veeravalli, S. V. 1994 Local isotropy in turbulent boundary layers at high Reynolds numbers. *J. Fluid Mech.* **268**, 333–372.

Sandham, N. D. & Howard, R. J. A. 1995 Statistics databases from direct numerical simulation of fully-developed turbulent channel flow. *Tech. Rep.* QMW-EP-1106. Department of Engineering, Queen Mary and Westfield College Rep.

Westbury, P. S. & Sandham, N. D. 1996 Analysis of coherent structures and energy transfer using discrete wavelets. *Tech. Rep.* QMW-EP-1111. Department of Engineering, Queen Mary and Westfield College.

Westbury, P. S., Sandham, N. D. & Morrison, J. F. 1998 Bursts and subgrid-scale energy transfer in turbulent wall-bounded flow. In *Advances in Turbulence VII* (ed. U. Frisch), pp. 23–26. Kluwer.